

Studies of the Effects of Actuator Errors on the HCIT/PIAA Contrast Performance

Erkin Sidick*, Stuart Shaklan, Amir Give'on, and Brian Kern
Jet Propulsion Laboratory, California Institute of Technology, 4800 Oak Grove Drive, Pasadena,
CA, USA 91109

ABSTRACT

The High Contrast Imaging Testbed Phase Induced Amplitude Apodization (HCIT/PIAA) coronagraph system at JPL relies on an Electric-Field Conjugation (EFC) wavefront correction algorithm to obtain the required high contrast. This algorithm works with one deformable mirror (DM) to estimate the electric-field to be controlled, and with one or multiple DM's to create a "dark-hole" in the image plane. We have investigated the effects of DM actuator errors on the efficiency of the EFC algorithm. The structural design of the optical system as well as the parameters of various optical elements used in the analysis are drawn from those of the HCIT/PIAA system that have been and will be implemented with one or two DM's. The simulation takes into account the surface errors of various optical elements. In this paper, we report our findings in the case of narrowband wavelength light.

Keywords: Coronagraph, high-contrast imaging, PIAA, pupil mapping, exoplanets

1. INTRODUCTION

The High Contrast Imaging Testbed Phase Induced Amplitude Apodization (HCIT/PIAA) coronagraph system at Jet Propulsion Laboratory [1] relies on a broadband wavefront correction algorithm called Electric-Field Conjugation (EFC) to obtain the required 10^{-10} contrast [2]. This algorithm works with one or multiple deformable mirrors (DM's) to create a "dark-hole" in a predefined region of the image plane where terrestrial planets would be found. It achieves the desired high contrast level in two stages. The first is the reconstruction stage. In this stage, the algorithm provides an estimate of the aberrated complex electric-field (e-field) in the image plane based on pairs of images taken at the final image plane using different DM configurations. The second is the correction or the e-field conjugation stage. In this stage the algorithm generates a correction based on the estimated e-field of the first stage. The correction is then applied to the DM actuators to null the image plane e-field in the predefined dark-hole region.

We have investigated the effects of the DM actuator errors on the efficiency of the EFC algorithm. Considered cases include random actuator gain errors, asymmetric actuator gain errors, the nonlinearity in DM actuator response to the applied control voltages, and bad (or dead) actuators. The structural design of the optical system as well as the parameters of various optical elements used in the analysis are drawn from those of the HCIT/PIAA system that have been and will be implemented with one or two DM's. The simulation takes into account the surface errors of various optical elements. The optical simulation algorithm uses MACOS (Modeling and Analysis for Controlled Optical Systems) as its analytic tool [3]. Hence it is capable of performing full three-dimensional near-field diffraction analysis on HCIT's optical model. This paper presents results on the effects of DM actuator gain errors on the estimation and the control of the e-field at the final image-plane of HCIT/PIAA when the light source is a narrow-band beam. The dependence of the broadband contrast performance of the HCIT/PIAA system on various errors, such as actuator errors, optical surface errors and rigid-body errors, will be studied and reported elsewhere.

2. BACKGROUND

The study in this paper is the continuation of the work reported in Ref. [1]. Therefore, the layout of the optical system and the phase errors of the five optics used in this study are identical to those described in Ref. [1]. The main difference in the optical model parameters used in this paper and in Ref. [1] are the following: (1) In this paper we treat the case of

*Erkin.Sidick@jpl.nasa.gov; Phone 1 818 393-7585; Fax 1 818 393-9471; www.jpl.nasa.gov

an optical system with only one DM. This is achieved by replacing DM2 with a flat mirror (see Fig. 1 in Ref. [1]). (2) We use a new apodization profile to be explained below. (3) We use a system aperture diameter $D=30\text{mm}$. But the input beam is still a narrowband light having a center wavelength of $\lambda_0=800\text{nm}$.

2.1 DM Actuator Model

The characteristics and the physical parameter of the 1024-actuator (or 32×32 actuator) DM used in this study are identical to those described in detail in Ref. [4]. Therefore, they will not be explained here. In this subsection, we briefly explain the optical model of an actuator used in our simulations. When a voltage V is applied to an actuator, its height increases or decreases, this in turn causes an upward or downward bending of the small area of the DM facesheet just above that actuator. Theoretically, for the Xinetics DM used on our testbed, the actuator command $V = 0\text{V} - 100\text{V}$ changes the actuator height by $h(V) = 0\text{nm} - 500\text{nm}$. For convenience, we assume $V = -50\text{V}$ to $+50\text{V}$ for the actuator command and $h(V) = -250\text{nm}$ to $+250\text{nm}$ for the actuator height in our simulations. The exact behavior of the $h(V)$ versus V curve of a mounted actuator is not known to us. But some preliminary measurements carried out at JPL indicate that the $h(V)$ versus V curves are not linear and their shapes are different for different actuators. We will study the several cases of the $h(V)$ versus V curves in this paper. The DM actuator model used in our simulations was developed at JPL based on the information provided by Xinetics, and is explained in Figs. 1(a-c) with Act(17,17) as an example, where we used Act(m,n) to denote an actuator having a row-number m and a column-number n , respectively. In an ideal case, $h(V) = \eta V$ with $\eta = 5\text{nm/V}$. The results in Figs. 1(a-c) correspond to $V = 2\text{V}$ and $h(V) = 10\text{nm}$. In these figures, the RMS and PV are the root-mean-square and the peak-to-valley values of the corresponding surface map, respectively.

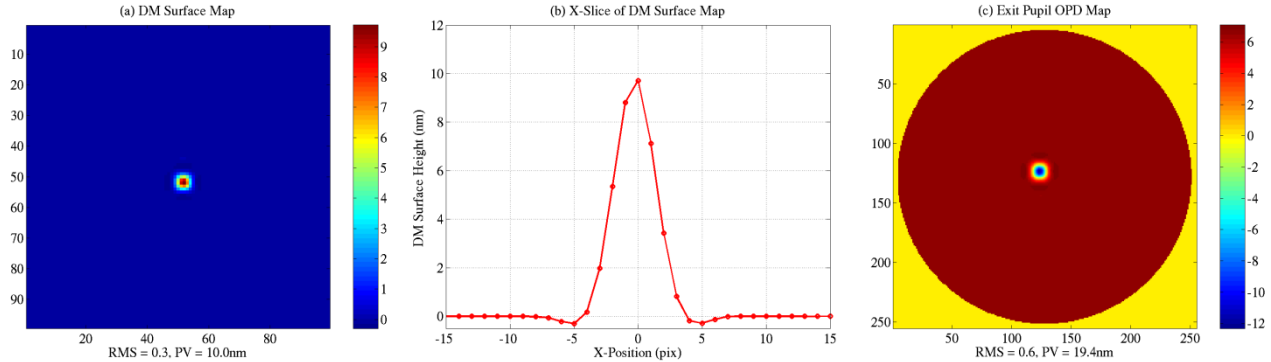


Figure 1. DM surface and exit pupil optical path difference (OPD) parameters when Actuator(17,17) is poked with $V = 2\text{V}$.

(a) 99x99 pix DM surface map, (b) its x-slice, and (c) the corresponding exit pupil OPD. The RMS and PV are the “root-mean-square” and the “peak-to-valley” values of the corresponding surface map, respectively.

2.2 Definition of Half Dark-Hole Area

For the current optical system with only one DM, we carry out wavefront control (WFC) over a half dark-hole region having a rectangular boundaries from $x/f = 5\lambda/D$ to $11\lambda/D$ in the x-direction and from $y/f = -10\lambda/D$ to $10\lambda/D$ in the y-direction. For a simulation grid size of 512×512 pixels, this gave an e-field vector, \vec{e} , having a size of 2992×1 pixels. There are a total of 1024 DM actuators in the current 1-DM system, but we excluded the actuators with zero or very weak influences, thus reducing the number of the actuators used to 984. We will keep track of the following three contrast parameters in this paper: (i) C_b , the mean contrast inside a “Big” rectangular region from $x/f = 5\lambda/D$ to $10\lambda/D$ and from $y/f = -10\lambda/D$ to $10\lambda/D$. (ii) C_s , the mean contrast inside a “Small” rectangular region from $x/f = 5\lambda/D$ to $6\lambda/D$ and from $y/f = -1\lambda/D$ to $1\lambda/D$. (iii) C_m , the “Maximum” contrast value inside the small rectangular region defined above. The nominal values of these parameters obtained for the error-free optical system without conducting any wavefront control are $C_b = 1.34\text{E}-5$, $C_s = 8.85\text{E}-5$, and $C_m = 1.51\text{E}-5$, respectively. When the phase errors of the five optics are included in simulation, the above contrast values change to $C_b = 1.64\text{E}-5$, $C_s = 3.21\text{E}-5$, and $C_m = 6.63\text{E}-5$, respectively. We will include the phase errors of the five optics in this study unless otherwise stated.

2.3 Amplitude Drooping

The illuminating beam of the current system exhibits a small level of amplitude-drooping at the exit pupil, but our simulations have shown that such amplitude-drooping does not have any adverse effect on the contrast performance of the HCIT/PIAA. Therefore, this effect will not be taken into account in our simulations.

2.4 Wavefront Control Algorithm and Approach

We will use the EFC algorithm for our WFC, and calculate the gain matrix using the “actuator regularization” method explained in Refs. [1-2]. We use an optimized sensitivity matrix $\tilde{\mathbf{S}}$ and an optimized set of four actuator regularization values, $\gamma_{wu} = [100 \ 1000 \ 2000 \ 4000]$, with the corresponding WFC iteration numbers listed in the same order, $N_{\text{WFC}} = [150 \ 25 \ 25 \ 25]$. That is, in a typical numerical WFC operation, the WFC process is completed in four phases with four different γ_{wu} values in the order given above, each with a different WFC iteration number also given above. The description of the process by which these optimum $\tilde{\mathbf{S}}$ and γ_{wu} were obtained is beyond the scope of this paper and will be presented in a separate publication.

2.5 Apodized Pupil Profile and WFC Efficiency

The apodized pupil profile used in this study is shown by the red-curve in Fig. 2(a). This is the profile currently being used on the HCIT/PIAA testbed and corresponds to the output of a PIAA unit without a post-apodizer. We call it “PIAA-A” in this paper. One characteristic of this PIAA profile is that there is still substantial residual light near the edges of the pupil. For that reason, including and not including the optics phase errors in simulation do not make much difference in the three types of contrast values, as explained in subsection 2.2, and the WFC process requires a large number of control iterations to achieve the ultimate dark-hole level, as is shown with a red-curve in Fig. 2(b), where the values of C_b is shown as a function of control iteration number. The phase errors of all five optics were included in this simulation. After 225 control iterations, we achieve a narrow-band half-dark hole having only $C_b = 1.58\text{E} - 10$. It must be pointed out that utilizing a post-apodizer in the PIAA unit dramatically improves this situation. For example, shown with a blue-curve in Fig. 2(a) is another PIAA profile referred to as “PIAA-B” in this paper. It corresponds to the output of a PIAA unit having a post-apodizer, and under the same condition of rad-curve in Fig. 2(b), this profile yields $C_b = 3.68\text{E} - 12$ after only 50 control iterations. The before- and the after-control PSFs corresponding to the above two PIAA profiles are shown in Figs. 3(a-d). These PSF maps are included here as examples of the numerical PSFs obtained in the current HCIT/PIAA system. The MACOS simulation tool allows us to calculate the complex e-field in the final focal plane directly, and we obtained the results presented in this sub-section that way, that is, without using the four-probe e-field estimation routine [2]. However, we will use the four-probe e-field estimation routine in the remaining part of this paper unless otherwise stated.

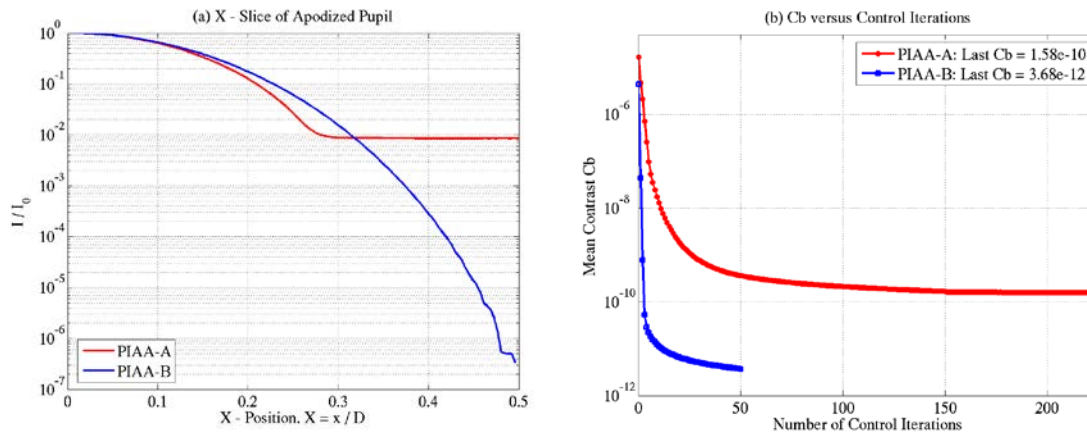


Figure 2. (a) Two apodization profiles, of which the red profile is used on the current HCIT/PIAA system, and (b) the corresponding contrast value C_b versus control iteration number.

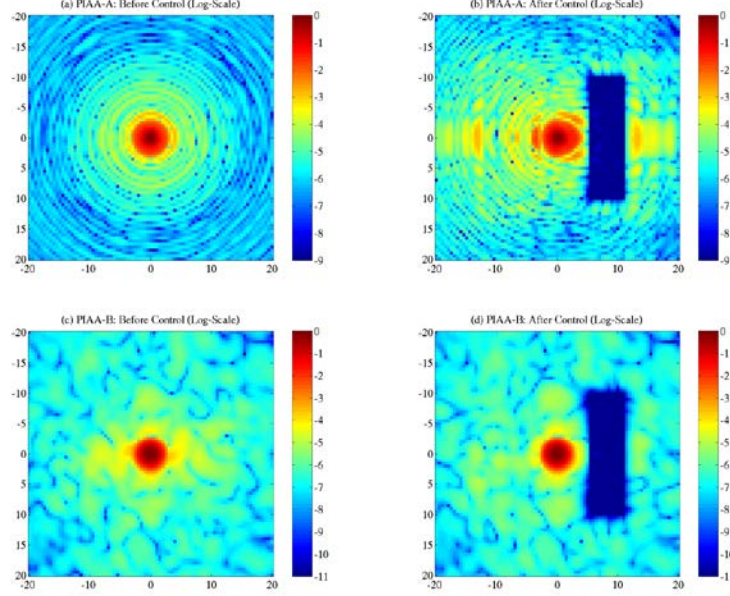


Figure 3. The calculated before- and after-control PSFs (central square portion only) corresponding to the current HCIT/PIAA testbed model utilizing the apodized pupil profiles PIAA-A and PIAA-B, respectively. The horizontal and the vertical axes are the field angles having a unit of λ/D .

3. SIMULATION RESULTS

3.1 Ideal Actuators

As explained in sub-section 2.1, ideal actuators have

$$h_i(V_i) = \eta V_i, \quad \eta = 5\text{nm/V}, \quad -50\text{V} \leq V_i \leq +50\text{V}, \quad (1)$$

where the subscript i corresponds to the actuator number. In this case, we obtain a result of C_b versus control iteration number similar to the red-curve in Fig. 2(b), and the pre- and post-control PSFs similar to Figs. 3(a-b), respectively (The results in Fig.2 and Fig. 3 were obtained without using the e-field estimation routine, whereas the ones in this subsection were obtained using the e-field estimation routine). The contrast values after 225 control iterations are $C_b = 1.61\text{E} - 10$, $C_s = 4.92\text{E} - 11$, and $C_m = 1.42\text{E} - 10$, respectively. The corresponding exit pupil OPD maps and the DM actuator height map are shown in Figs. 4(a-c), respectively. As before (see Ref. [1]) and as is expected, the WFC process does not minimize the exit pupil wavefront error (WFE) in the current case, instead, it re-arranges the WFE to create the desired dark-hole. The values of the actuator heights after 225 control iterations have a range of roughly -150nm to +100nm, as shown in Fig. 4(c).

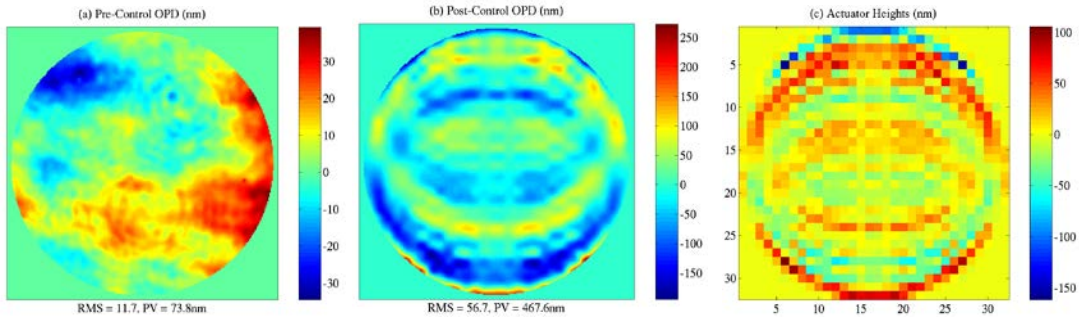


Figure 4. (a) Exit-pupil OPD map before control, (b) after control, and (c) the actuator height map after 225 control iterations.

3.2 Linear Actuator response with Random Slope (or Gain) Errors

Next, we investigate a case where all of the actuators have linear responses to the command voltage but with slightly different slopes, that is,

$$h_i(V_i, \sigma_u) = (1 + \sigma_u f_{nri}) \eta V_i, \quad \eta = 5\text{nm/V}, \quad -50\text{V} \leq V_i \leq +50\text{V}, \quad (2)$$

where f_{nri} is a normally-distributed random-number variable. Its values can be obtained using a seeded Matlab function, *randn.m*. Because f_{nri} has a standard-deviation (STD) of 1.0, the factor $\sigma_u f_{nri}$ corresponds to the actuator response slope error with an STD of σ_u . In our simulations, we introduced the same errors into both the four-probe e-field estimation and the EFC-based WFC operations. Figure 5(a) shows one realization of f_{nri} values of all 984 active actuators, and Fig. 5(b) shows the C_b versus control iteration number results corresponding to four σ_u values indicated on the figure legends. As we can see, the C_b of the $\sigma_u = 0.3$ case increases and oscillates first, and then decreases, but it decreases monotonically in the remaining three cases. Even though the differences in the last C_b values are negligible for all practical purposes, the last C_b value gets slightly improved with the increased σ_u value in this particular case of slope errors. Such a result is completely unexpected.

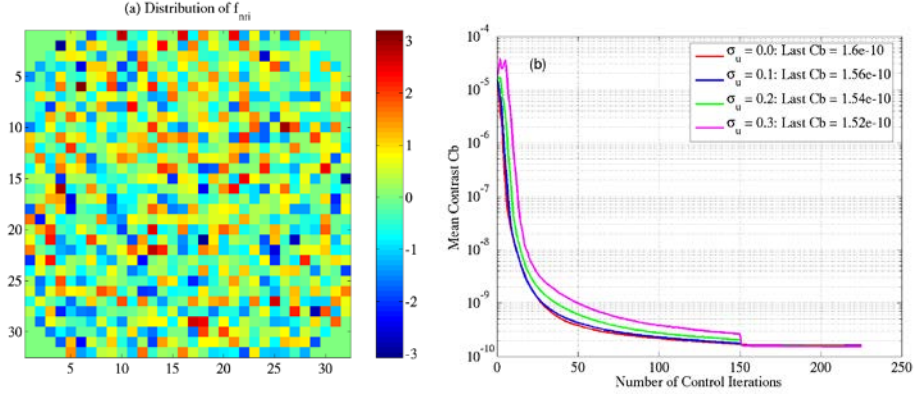


Figure 5. (a) The distribution of one f_{nri} realization used in the current simulations. (b) C_b versus control iteration number curves obtained with four different σ_u values.

In order to understand what leads to the above results, we examined the behavior of the final focal-plane e-field in response to the applied actuator command. The system influence functions (or sensitivity matrix) used in this study was obtained by changing the command voltage of each actuator from 0V to +1V (or by changing the input actuator height from 0nm to 5nm), and dividing the resultant differential e-field vector by $\Delta V = 1\text{V}$ (or $\Delta h = 5\text{nm}$). Let us denote such an influence function vector with $\vec{s}_i(5\text{nm})$, where the subscript i corresponds to the actuator number as before. When we conduct WFC to create a dark hole, the resulted actuator heights of the active actuators will differ from 5nm, in some cases by a lot, as is seen from Fig. 4(c). Then, how accurate the $\vec{s}_i(5\text{nm})$ are at other actuator height positions? To find an answer for this question, for Act(17,17), we took the pseudo-inverse of $\vec{s}_i(5\text{nm})$ to obtain a gain row-vector, $\vec{g}_i(5\text{nm})$, and reconstructed the actuator heights at other input actuator height values as

$$h_{\text{reci}}(h) = \vec{g}_i(5\text{nm}) \times \vec{e}_i(h), \quad (3)$$

where $\vec{e}_i(h)$ is a differential e-field column-vector defined in Ref. [1]. It is obtained from the e-field at some non-zero h -value minus the e-field at $h = 0\text{nm}$. The result of $h_{\text{reci}}(h)$ for Act(17,17) is shown in Fig. 6(a) with a red-curve. If we “turn off” the diffraction propagation completely and use only ray-tracing in our simulation, then we obtain the blue-curve. If the system had been linear, we would have obtained the green-curve. As we can see, the current system is almost linear in the 0nm to +100nm actuator height range, but highly nonlinear and its slope is always < 1 in the 0nm to -100nm range. In this case, an input of -100nm produces only a -66nm effect. Figure 6(b) shows the $\left| \frac{[\vec{E}(V) - \vec{E}(0V)]}{V} \right|$ maps when $V = -20\text{V}$ and $+20\text{V}$ (or $h = -100\text{nm}$ and $+100\text{nm}$), respectively. As is seen, the diffraction-propagation

makes the e-fields at $h = -100\text{nm}$ and $+100\text{nm}$ fairly asymmetric. A careful examination of the actuator heights in Fig. 4(c) revealed that 51.1% of them have negative values, whereas the values of f_{nri} corresponding to those negative actuators (that is, the actuators having negative height values) split almost 50%-50%. For that reason, in the current particular case of f_{nri} , the slope errors slightly improved the value of C_b .

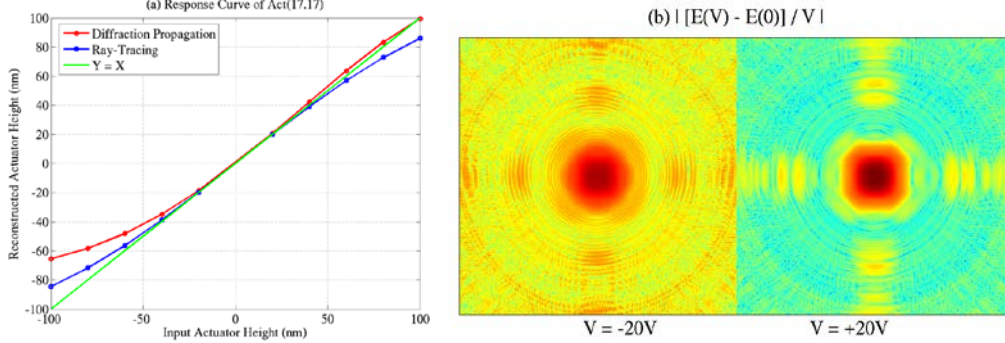


Figure 6. (a) Reconstructed actuator height versus input actuator height. (b) Magnitude of the normalized differential e-fields when $V = -20\text{V}$ and $+20\text{V}$, respectively.

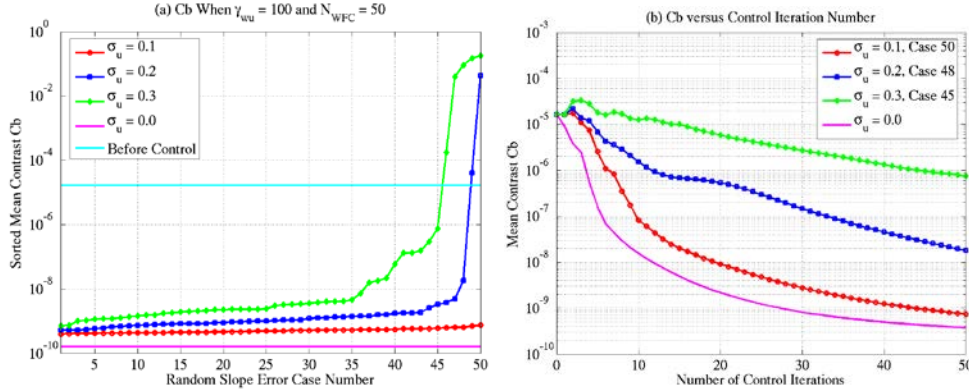


Figure 7. (a) Values of C_b after 50 control iterations carried out with $\gamma_{wu} = 100$ and corresponding to 50 sets of random slope error realizations. C_b of $\sigma_u = 0$ is the one obtained with $N_{WFC} = 225$. (b) C_b versus control iteration number, where the case numbers on the figure legends correspond to the horizontal axis of part (a).

We carried the above simulations for another 50 realizations of the slope errors with $\sigma_u = 0.1, 0.2, 0.3, \gamma_{wu} = 100$ and $N_{WFC} = 50$, and obtained the results shown in Fig. 7(a), where the last values of C_b were sorted first, then plotted as a function of slope error case number. When $\sigma_u = 0.3$, in the five cases out of 50 (or in the 10% cases), the e-field estimation and control operations fail and result in C_b values larger than the pre-control value. For those five cases we tried to use much less aggressive actuator regularization values, such as $\gamma_{wu} = 5000$, but still could not create a dark hole. We got similar results in two $\sigma_u = 0.2$ cases, Cases 49 and 50. As is seen from Fig. 7(b), the random slope errors in actuator response curves slow down the efficiency of WFC in all “good” cases, i.e., the cases where C_b becomes smaller than its pre-control value. We can expect that, in some of those “good” cases, the C_b value will never get as good as in the case of $\sigma_u = 0.0$.

3.3 Linear Actuator Response with Asymmetric Slope Errors

In this sub-section we consider a different type of actuator errors in which the actuator response curves of all active actuators are linear but have different slopes for positive and negative commands. Mathematically, this can be expressed as

$$h_i(V_i, \delta_i) = (1 + \delta_i)\eta V_i, \quad \eta = 5\text{nm/V}, \quad -50\text{V} \leq V_i \leq +50\text{V}. \quad (4)$$

We consider two types of scenarios under this category. They are “Negative Slope Errors” and “Positive Slope Errors”, respectively, are mathematically represented by

$$\text{Negative Slope Errors : } \delta_i = \begin{cases} \delta_{\text{neg}}, & V_i \leq 0V \\ \delta_{\text{pos}} = 0, & V_i > 0V \end{cases} \quad \text{Positive Slope Errors : } \delta_i = \begin{cases} \delta_{\text{neg}} = 0, & V_i \leq 0V \\ \delta_{\text{pos}}, & V_i > 0V \end{cases} \quad (5)$$

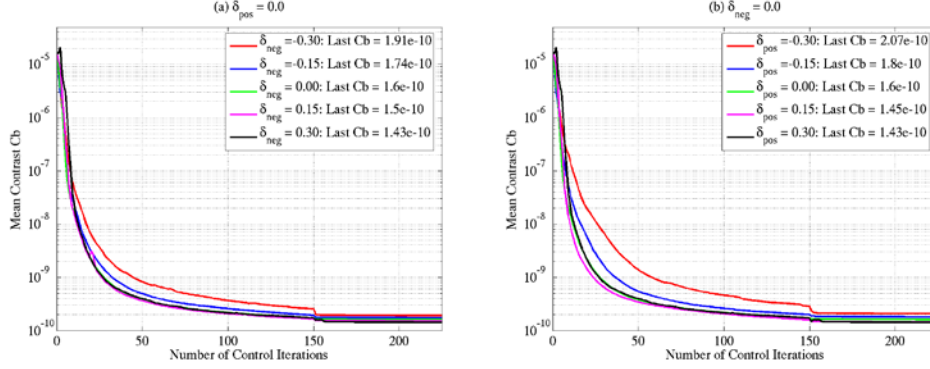


Figure 8. C_b versus control iteration number when the actuator response curves have (a) negative slope errors and (b) positive slope errors, respectively.

Based on the information presented in the previous sub-section, the results in Fig. 8(a) can be easily understood. However, as is seen from Fig. 8(b), we get better C_b results with the increased positive slope errors also, just as in the case of negative slope errors. We believe this is caused by the combination of several factors, such as the choices on γ_{wu} and N_{WFC} , as well as the ultimate actuator height values required to create a dark hole in the current particular case of optical system.

3.4 Nonlinear Actuator Response with Random Slope Errors

In general, one can expect that the h versus V curve of each actuator is nonlinear and these curves are different for different actuators. Some preliminary measurements of the actuator response curves [5] have indeed exhibited the evidence of such behavior, as is shown in Figs. 9(a-b) (Note that a command voltage axis stretch of 0 – 100V is used in these two figures). Experimental details of these measurements are beyond the scope of this paper and will not be presented here. Based on the knowledge learned from these measurements, we constructed a model of actuator nonlinear response curves with some random slope errors, which is

$$\begin{aligned} h_i(V_i, \delta_i) &= (1 + \delta_i)h(V_i), \quad -50V \leq V_i \leq +50V \\ h(V_i) &= a_5V_i^5 + a_4V_i^4 + a_3V_i^3 + a_2V_i^2 + a_1V_i + a_0, \end{aligned} \quad (6)$$

$$\begin{aligned} a_5 &= 1.3240845E - 7 \\ a_4 &= -2.49561496E - 6 \\ a_3 &= -1.06394116008E - 3 \\ a_2 &= 5.8245995026E - 3 \\ a_1 &= 5.48435803758743 \\ a_0 &= 0 \end{aligned}$$

In Eqn. (6), δ_i are random numbers obtained from the Matlab function *randn.m* and re-scaled the negative and positive parts separately such that $-0.3 \leq \delta_i \leq +0.3$. This range of the δ_i values roughly corresponds to the dh/dV data in Fig. 9(b) at $V = 30V$. Figures 10(a-b) show the several examples of h and dh/dV versus input command curves obtained using Eqn. (6).

We carried out WFC simulations with $\gamma_{\text{wu}} = 100$ and $N_{\text{WFC}} = 50$ for 50 sets of random δ_i realizations, and obtained the result shown in Fig. 11(a), where the last values of C_b were sorted first, then plotted as a function of slope error case number. In this figure, there are 20 cases where $C_b(\sigma_i \neq 0) \leq C_b(\sigma_i = 0)$, or, in another words, the C_b gets slight

improvement or stays the same as compared to the case of $\sigma_i=0$. We believe the same mechanism as explained in Sub-section 3.2 is responsible for the slight improvement in C_b . In the remaining 30 cases, we get $C_b(\sigma_i \neq 0) > C_b(\sigma_i=0)$. In Fig. 11(b), we compared the C_b versus control iteration number curves of Cases 1 and 50 with the similar curve corresponding to $\sigma_i=0$. As we can see from this figure, the WFC process becomes less efficient in the cases where $C_b(\sigma_i \neq 0) > C_b(\sigma_i=0)$. If we conduct a full-sequence of WFC with $\gamma_{wfc} = [100 \ 1000 \ 2000 \ 4000]$ and $N_{WFC} = [150 \ 25 \ 25 \ 25]$ for Case 50, we obtain $C_b = 1.87E-10$, $C_s = 4.89E-11$, and $C_m = 1.33E-10$, respectively. These results are very close to those obtained with $\sigma_i=0$ (see Sub-section 2.1).

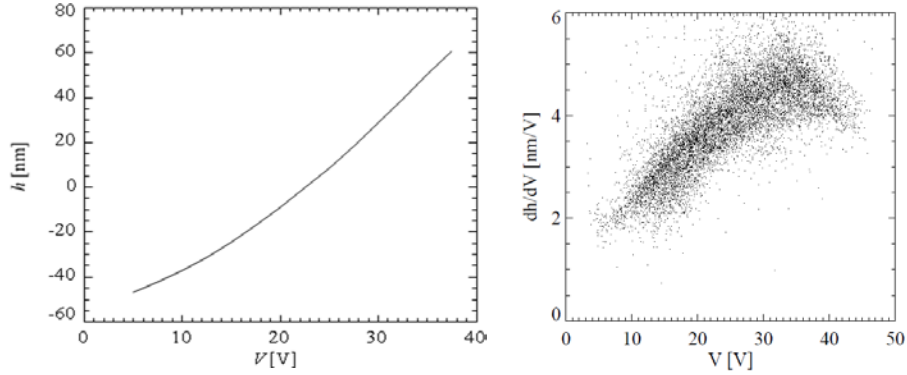


Figure 9. (a) Measured actuator height versus input command curve of one actuator, and (b) measured dh/dV versus input command data of ~ 1000 actuators. What are shown in the y -axis of part (a) are the relative values of h .

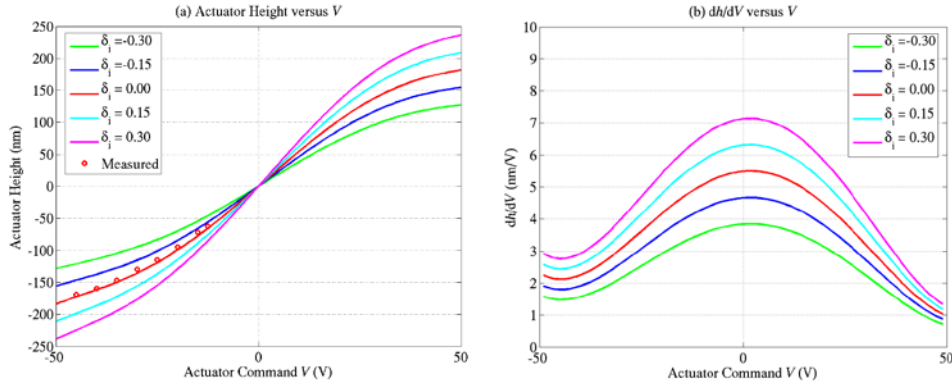


Figure 10. Several examples of (a) actuator height and (b) dh/dV versus input command curves obtained using Eq. (6).

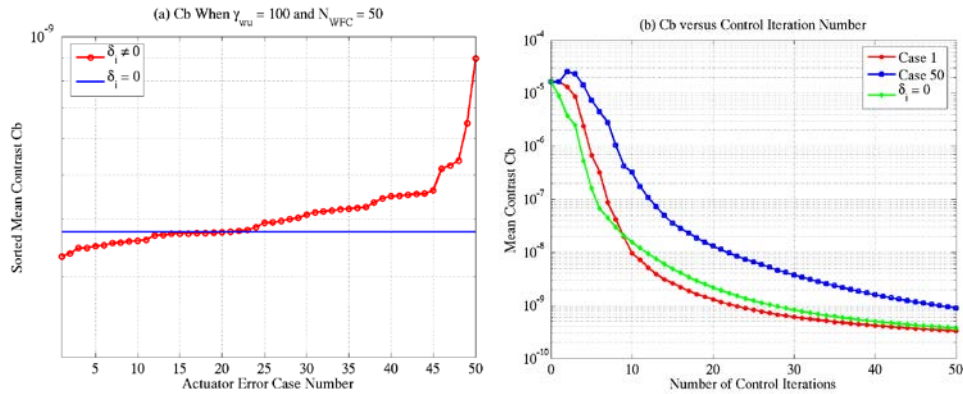


Figure 11. (a) Values of C_b after 50 control iterations carried out with $\gamma_{wfc} = 100$ and corresponding to 50 sets of σ_i realizations. (b) C_b versus control iteration number, where the case numbers on the figure legends correspond to the horizontal axis of part (a).

3.5 Dead Actuators

Finally, we examined a new situation where some of the active actuators are not responsive to the applied commands. We call such actuators as “dead actuators” in this paper. In the current simulations, for the optical system with all five phase errors and the actuators whose h - V characteristic is given by Eqn. (1), we obtained actuator command solutions in each WFC iteration as usual, but set the command value or values of randomly selected one, two or three actuators to 0V when performing the next WFC iteration. The sorted minimum values of the C_b are shown as a function of dead actuator case number in Fig. 12(a) for three different numbers of dead actuators, N_{dead} , and for a total of 50 dead actuator realizations. Figure 12(b) shows the C_b versus control iteration number curves corresponding to the worst cases in Fig. 12(a) for all three values of N_{dead} except $N_{\text{dead}} = 3$. In the latter case, we failed to create a dark hole even with a much more conservative value of actuator regulation parameter, $\gamma_{\text{wu}} = 4000$. Therefore, we did not include the result of the C_b corresponding to that case in Fig. 12(a), and presented the curve corresponding to the Case 49 of $N_{\text{dead}} = 3$ instead in Fig. 12(b). Figures 13(a-c) show the locations of the dead actuators randomly selected in the above simulations. By direct observation, we did not notice anything special about the Case 50 of $N_{\text{dead}} = 3$, as shown in Fig. 14, where the locations of the three dead actuators are indicated with red-square marks on top of the actuator height maps corresponding to the case of $N_{\text{dead}} = 0$ and obtained at the end of the usual 225 WFC iterations.

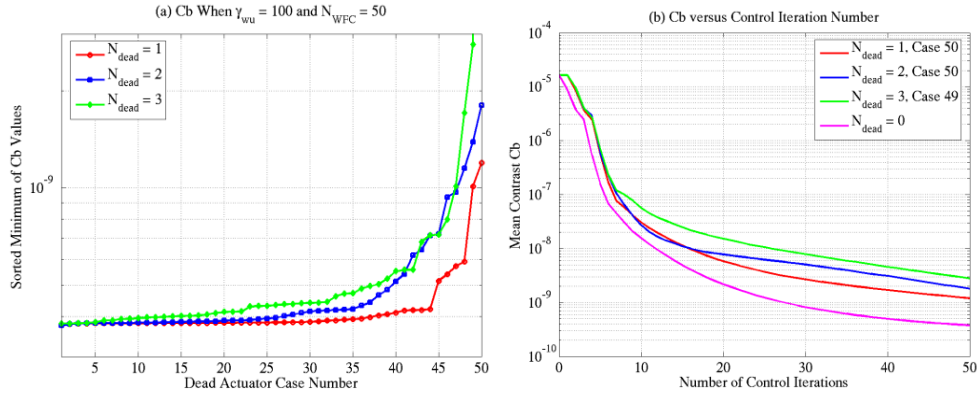


Figure 12. (a) Values of C_b after 50 control iterations carried out with $\gamma_{\text{wu}} = 100$ and corresponding to one, two and three randomly selected dead actuators. In these simulations, the values of all actuator commands were obtained as usual (or using all influence functions), but the command values of those dead actuators were set to 0V before carrying out the next WFC iteration. (b) C_b versus control iteration number, where the case numbers on the figure legends correspond to the horizontal axis of part (a).

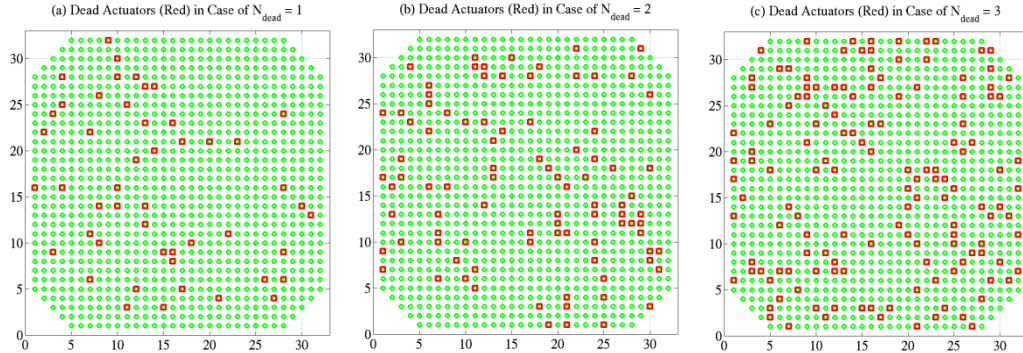


Figure 13. Locations of dead actuators randomly selected in the current simulations, with (a) $N_{\text{dead}} = 1$, (b) $N_{\text{dead}} = 2$, and (c) $N_{\text{dead}} = 3$, respectively, where N_{dead} denotes the number of dead actuators. The green-square marks in all three parts show the locations of all the active actuators.

Again, as we can see from Figs. 12(a-b), the effect of the one, two or three dead actuators, at least for the most cases considered here, is to slow down the process of WFC.

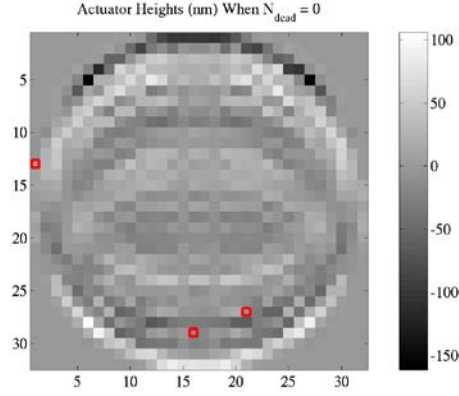


Figure 14. Actuator heights of the $N_{\text{dead}} = 0$ case obtained after 225 WFC iterations and the locations of the three dead actuators corresponding to $N_{\text{dead}} = 3$, Case 50 in Figs. 12 and Fig. 13(c).

3.6 Summary of Results

The results of all the actuator error cases studied in this section are summarized in Table 1.

Table 1. Summary of the values of three types of contrast, C_b , C_c and C_m , obtained before and/or after wavefront control when introducing different types of errors into the PIAA/HCIT system.

Case #	Error Parameter	Value of Error Parameter	Remarks	Range of Good Case C_b Values	Total Number of Cases Studied	Number of Good Cases
0.1	Nominal		Before Control	1.3E-05	1	1
0.2	Figure Error	12 nm RMS	Before Control	1.6E-05	1	1
			After Control	1.6E-10	1	1
1.1	σ_u	0.1	Linear $h(V)$ with random slope errors	4.0E-10 - 7.4E-10	50	50
1.2		0.2		5.2E-10 - 1.8E-08	50	48
1.3		0.3		7.1E-10 - 7.6E-07	50	45
2.1	δ_{neg}	-0.30	Linear $h(V)$ with slope errors at $V < 0V$	1.9E-10	1	1
2.2		-0.15		1.7E-10	1	1
2.3		0.15		1.5E-10	1	1
2.4		0.30		1.4E-10	1	1
3.1	δ_{pos}	-0.30	Linear $h(V)$ with slope errors at $V > 0V$	2.1E-10	1	1
3.2		-0.15		1.8E-10	1	1
3.3		0.15		1.5E-10	1	1
3.4		0.30		1.4E-10	1	1
4	δ_i	-0.3 to 0.3	Nonlinear $h(V)$ with random slope errors	3.3E-10 - 9.0E-10	50	50
5.1	N_{dead}	1	Linear $h(V)$, and 1-3 actuators are set to $h(V) = 0\text{nm}$ in e-field estimation & control	3.8E-10 - 1.2E-09	50	50
5.2		2		3.7E-10 - 1.8E-09	50	50
5.3		3		3.8E-10 - 2.8E-09	50	49

4. CONCLUSION

The behavior of the actuators of the deformable-mirrors (DMs) utilized on the HCIT/PIAA testbed plays crucial role in its contrast performance. In order to gain some general understanding about the potentials and the limitations of the current single-DM HCIT/PIAA system, we have examined through modeling and simulations the effects of some common actuator errors on the estimation and the EFC-based control of the e-field over a half-dark hole region. Considered cases include random slope errors of actuator linear response curves, asymmetric slope errors of actuator linear response curves, nonlinear response curves of actuators with random slope errors, and 1-3 dead actuators. We have shown that, within the extent of the actuator errors considered in this paper, the random, 30% slope errors in the linear actuator response curves have the largest negative impact on the contrast performance of the HCIT/PIAA. In this case, we failed to create a half-dark hole in the 10% of the time, and the WFC efficiency was reduced in the remaining 90% of the time, in some cases very severely. Most of the other actuator errors considered in this paper have shown to be tolerable. This study has been limited to a narrowband input light and a perfect PIAA unit. We plan to extend this work to broadband input light and imperfect mapping system in our future studies.

This work was carried out at the Jet Propulsion Laboratory, California Institute of Technology, under contract with the National Aeronautics and Space Administration.

REFERENCES

1. Erkin Sidick, John Z. Lou, Stuart Shaklan, and Marie Levine, "Performance Sensitivity Studies on the PIAA Implementation of the High-Contrast Imaging Testbed," Proc. SPIE, **7440**, 74400I (2009), and the references therein.
2. Amir Give'on *et al*, "Broadband wavefront correction algorithm for high-contrast imaging system," Proc. SPIE, **6691**, 66910A (2007).
3. *Modeling and Analysis for Controlled Optical Systems User's Manual*, Jet Propulsion Laboratory, California Institute of Technology, Pasadena, CA.
4. John T. Trauger, Chris Burrows, Brian Gordon, Joseph J. Green, Andrew E. Lowman, Dwight Moody, Albert F. Niessner, Fang Shi, and Daniel Wilson, "Coronagraph contrast demonstrations with the high-contrast imaging testbed," Proc. SPIE, **5487**, 1330, 2004.
5. Brian D. Kern, Jet Propulsion Laboratory, California Institute of Technology, Pasadena, California 91109 (personal communications, 2009).